applied sciences

MDPI

Article

Experimental Study on Freezing Front Model of Alpine Tunnel under Wind Field

Zhiqiang Li [1], Jinpeng Zhao [2], Lulu Liu [2,3,*] and Zhe Li [2]

[1] School of Civil Engineering, Weifang University, Weifang 261061, China
[2] School of Highway, Chang'an University, Xi'an 710064, China
[3] State Key Laboratory for Geomechanics and Deep Underground Engineering, China University of Mining and Technology, Xuzhou 221116, China
* Correspondence: liululu@cumt.edu.cn; Tel.: +86-18651611376

Abstract: In order to study the freezing front characteristics of alpine tunnels under the condition of wind flow field and relying on the Osaka Mountain tunnel in Qinghai Province, the physical model test of an alpine tunnel was built. By using the Surfer software combined with the laboratory test data, the radial and longitudinal temperature variation trends of the tunnel were obtained, and the overall temperature vector graph of the tunnel was simulated; the radial and longitudinal evolutionary laws of a freezing front in an alpine tunnel under airflow conditions were systematically analyzed, and the radial and longitudinal governing equations of a freezing front in the tunnel model under airflow conditions were proposed. The results show that: With the decrease of the test air temperature, the thermonuclear area in the surrounding rock gradually shrinks, the frozen area of surrounding rock at the bottom of the arch gradually increases, and the frozen area of surrounding rock at the top of the arch gradually expands to the interior of the mountain. The influence degree of ventilation on the longitudinal and radial temperature distribution of the tunnel is obvious, and the greater the wind speed, the greater the influence degree. In particular, the fluctuation range of the longitudinal temperature distribution of the tunnel is more extensive under the influence of ventilation. The freezing front distance in the inverted arch area is the largest, and the expansion distance of the freezing front in the wall foot area is obviously higher than that in the vault; the variation of the longitudinal freezing front at different positions of the tunnel shows parabolic attenuation and with an increase in tunnel depth, the trend of freezing front gradually eases and becomes stable and disappears; the three radial regions of the freezing front and the longitudinal quadratic parabola governing equations can predict the specific distribution characteristics of the freezing front at different depths of the tunnel.

Keywords: alpine tunnel; wind flow field; freezing front; model test

check for updates

Citation: Li, Z.; Zhao, J.; Liu, L.; Li, Z. Experimental Study on Freezing Front Model of Alpine Tunnel under Wind Field. *Appl. Sci.* **2023**, *13*, 824. https://doi.org/10.3390/app13020824

Academic Editor: Daniel Dias

Received: 3 December 2022
Revised: 1 January 2023
Accepted: 3 January 2023
Published: 6 January 2023

Copyright: © 2023 by the authors. Licensee MDPI, Basel, Switzerland. This article is an open access article distributed under the terms and conditions of the Creative Commons Attribution (CC BY) license (https://creativecommons.org/licenses/by/4.0/).

1. Introduction

With the increasing demand for transportation infrastructure construction in the Qinghai-Tibet Plateau and Northwest China, the construction scale of tunnels in high altitude cold regions is also expanding year by year, and the phenomenon of frost damage in railway and highway tunnels in cold regions is very common and serious [1,2]. Therefore, reducing tunnel frost damage has become a key scientific problem that needs to be solved urgently at present, and it is also a difficult and key point for scholars in the field of alpine tunnel engineering to study [3,4]. Especially in the extreme environment outside the tunnel, cold air enters the tunnel and repeatedly exchanges heat with the lining, resulting in severe frost damage to the tunnel lining, invert and drainage structure. These problems have been an issue for the operation management and safe driving of the alpine tunnel project [5,6].

Both domestic and foreign scholars have made a lot of achievements in the study of tunnels in cold areas under the action of wind flow field, most of which are based

on model tests and numerical simulation, etc. [7,8]. According to the research results, when the external air flows into the tunnel, the heat exchange between the air flow and surrounding rocks is the most intensive at the tunnel entrance; it then gradually decreases with the increase of ventilation distance, showing an inverted "V" variation trend on the whole. Krarti and Kreider (1996) obtained the analytical solution of the gas temperature field in the underground wind tunnel according to the law of conservation of energy [9]. He et al. (1996, 1999) predicted the freeze–thaw conditions of 46 surrounding rock tunnels in cold areas based on the combined convection–conduction model of 47 on-site temperature, atmospheric pressure and wind conditions [10,11]. Lai et al. (2002) deduced the analytical solution of the temperature field of circular tunnels and proposed the calculation method of the thermal insulation layer of tunnels in cold areas [12]. Tang and Wang (2007) analyzed the effect of temperature control on permafrost tunnels and established stable conditions related to melting depth and suitability for use in construction [13]. On the basis of thermal conductivity seepage theory, Xuefu et al. (2007) studied the influence of thermal insulation layers on controlling water leakage in permafrost tunnels by considering the coupling effect of seepage and temperature field, and carried out the three dimensional nonlinear analysis of the Kunlun mountain tunnel with and without an insulation layer [14]. Taking Zila mountain tunnel as an example, Zhou et al. (2021) studied the dynamic change of the temperature field during the operation of the tunnel by adopting the convection–conduction coupling transient heat transfer model [15]. In recent years, the finite element analysis method is often used to solve the heat transfer problem between tunnel surrounding rock and air [16]. Based on the heat transfer theory, Lai et al. (1999) used the finite element formula to make a nonlinear analysis of the temperature field, seepage field and stress field related problems in cold zone tunnels [17]. In order to study the influence of wind flow field on the temperature of tunnel-surrounding rock in cold areas, Tan et al. (2014) established the temperature field model of tunnel-surrounding rock, which includes the governing equation of surrounding-rock temperature, the governing equation of air temperature field in tunnel and the governing equation of wind flow in turbulent field [7]. On this basis, a numerical analysis method was adopted. The variation rule of surrounding-rock temperature field and specific insulation measures under ventilation conditions of Jialongla Tunnel in Xizang Province are discussed. Both mechanical ventilation and train-induced wind during train operation in the cold zone tunnel have a great influence on the temperature field inside the tunnel. Zhou et al. (2016) established an unsteady finite reference calculation model according to the unsteady finite difference equation of heat transfer and heat convection in the cold zone railway tunnel; the heat convection between air and tunnel wall and the heat conduction at the interface between surrounding rock and different materials in the tunnel structure are studied [6].

In practical engineering, when determining the insulation material and the suitable range of grouting in alpine tunnels, the predicted scale of tunnel structure under freezing temperature must be determined by predicting the temperature field before construction, and the freezing front becomes an inevitable discussion object [18,19]. As an important reference for thermal insulation design of alpine tunnels, freezing front has important guiding value for thermal insulation construction of alpine tunnel engineering. The current research results on the freezing front of alpine tunnels need to be explored further, as the existing research mainly focuses on single tube freezing and a small part of frozen soil freezing. The single-tube freezing theory considers the freezing point of soil, proposes the freezing front and considers that the temperature at the front is constant. This theory is only applicable to the solution of the freezing radius before the freezing front is closed, while the flat plate freezing theory is needed for the freezing radius after the freezing front is closed. The main reason is that the diameter of the freezing tube can be ignored in the calculation of the single-tube freezing problem. Thus, it can be simplified into a linear heat source model with analytical solutions, and the setting of a frozen soil temperature boundary can be simplified into a flat plate theory and the movement law of freezing front with freezing time can be obtained. Lunardini and Varotta (1981), Li and Xia (2004),

Jiang et al. (2009) proposed an analytical solution of the freezing temperature field of a single tube under the condition of a constant heat flow boundary [20–22]. Zhou and Zhou (2012) established an analytical solution to the single pipe freezing temperature field considering the presence of some unfrozen water in the frozen soil [23]. Cai et al. (2019) established an improved ground frost heave analysis and prediction method based on the formation process of freezing front in combination with the analysis and prediction proposed by Cai et al. (2014) [24,25]. In order to obtain the distribution law of freezing front under tunnel ventilation in cold regions, Liu et al. (2018) carried out model tests under different air temperatures and inlet wind speed, and established the radial three domain control equation and the longitudinal parabolic control equation of the freezing front [26]. The accuracy of the equation was verified by comparing the research results with the field measurement results. Cai et al. (2018) established the analytical solution of the single tube freezing temperature field considering the constant soil freezing temperature and freezing tube wall temperature [27]. The finite element program Abaqus was used to conduct numerical simulation of the single tube liquid nitrogen freezing temperature field, and the functional relationship between the freezing front radius, freezing time and freezing temperature was obtained. However, in practice, the overall radius of the tunnel section is large, the longitudinal temperature in the tunnel is different, and the temperature of the section cannot be ignored, so it is difficult to obtain the analytical solution to the freezing front.

At present, it is difficult to carry out field research on the freezing front of tunnels in alpine areas, and the physical model test can be used as an important means to obtain test data of freezing front research because of various simulated working conditions and convenient operation and construction. Taking the Osaka Mountain Tunnel in Qinghai Province as an example, this paper establishes a physical model of the cold tunnel, and systematically analyzes the radial and longitudinal evolution laws of the freezing front of the cold tunnel under the condition of air flow field. The radial three zone control equation and the longitudinal quadratic parabola control equation of the freezing front of the tunnel model under ventilation conditions are determined.

2. Physical Model Test Design

2.1. Model Test Equipment and Main Parameters

2.1.1. Freezing Devices

The freezing instrument used in this model test is the XT5710 frozen soil model test freezing system of the National Engineering Laboratory of Coal Mine Deep Well Construction Technology of Anhui University of Science and Technology. Figure 1 shows the power system and external circulation system.



(**a**) (**b**)

Figure 1. Power system and external circulation system: (**a**) Power system; (**b**) External circulation system.

2.1.2. Sensor

In this model test, 354 temperature sensors were used, all of which were K-type nickel chromium nickel silicon micro thermocouple with high sensitivity. Using a FY-KFS series hot-wire pipe wind speed sensor can achieve small air volume measurements and maintain high accuracy.

2.1.3. Test Data Acquisition Equipment

The temperature data acquisition instrument used in the model test is the TDS-303 type data acquisition instrument produced by Tokyo Measuring Instrument Company, Tokyo, Japan, and the wind speed data acquisition instrument is the FY-CJ2 type wind speed acquisition instrument.

2.2. Research on Tunnel Model Similarity

2.2.1. Similarity Ratio Design of Test Model

This tunnel model is a single-center circular tunnel. Considering the refrigerating laboratory area, model processability, economy, model operability and other factors, the final geometric reduction ratio of the tunnel section was determined to be 1:37. For a structure with a large tunnel slenderness ratio, if the overall scale model test is carried out, the variable rate model is required. According to the ventilation model test of the Hong Kong-Zhuhai-Macao Undersea tunnel conducted by Chang'an University, the variation rate in the length direction was set as k = 4, and the final model tunnel length was set as 3 m. The main design parameters of the tunnel prototype and model are shown in Table 1.

Table 1. Main design parameters of tunnel prototype and model.

Parameter	Prototype (cm)	Model (cm)	Similitude Ratio
Internal diameter	454	12.2	1:37
Primary lining thickness	40	1.08	1:37
Secondary lining thickness	68	1.84	1:37

2.2.2. Material Configuration

It is proposed to use C25 fine concrete to replace conventional concrete. The selection of fine concrete is due to the closeness between its thermal conductivity and C25 concrete. The mix ratio is water: cement: sand: gravel = 0.38:1:1.11:2.72.

The Osaka Mountain Tunnel site adopts polyurethane insulation board as insulation material. According to the energy conservation theorem, the thickness of polyurethane in the model is 1.5 mm. The average thermal conductivity of the main rocks is taken as the thermal conductivity of the rock surrounding the tunnel at the site, which is 2.474 W/(m·K). The thermal conductivity of model surrounding-rock is 1.551 W/(m·K). The mix ratio of surrounding rock material is water: sand: lime: stone: soil = 0.35:1.5:0.2:0.6:2.0. The thermal conductivity of model surrounding-rock is 1.551 W/(m·K), and the temperature similarity ratio of surrounding-rock materials is 1:1.37.

2.3. Model Test Design Scheme

2.3.1. Tunnel Mold Design and Lining Pouring

The test mold was welded with a 3 mm steel plate. The diameter of the inner template was 97 mm, and the diameter of the outer template was 140 mm. Bolt fixing ends should be used at the overlap between formworks to make the connection of formworks more stable. The internal insulation layer and temperature sensor of the lining should be fixed on the internal reinforcement mesh of the lining in advance, and the lining poured with equal thickness. Sprinkle water on the tunnel model for curing at regular intervals within a certain period after the completion of the model tunnel pouring.

2.3.2. Arrangement of Sensors

The temperature sensors for the tunnel model test in this cold region are arranged at 8 positions on the cross section: left foot of the wall, left side wall, arch, right side wall, right foot of the wall, lower right of the invert, lower middle of the invert and lower left of the invert. The specific arrangement is shown in Figures 2 and 3 (Unit: mm).

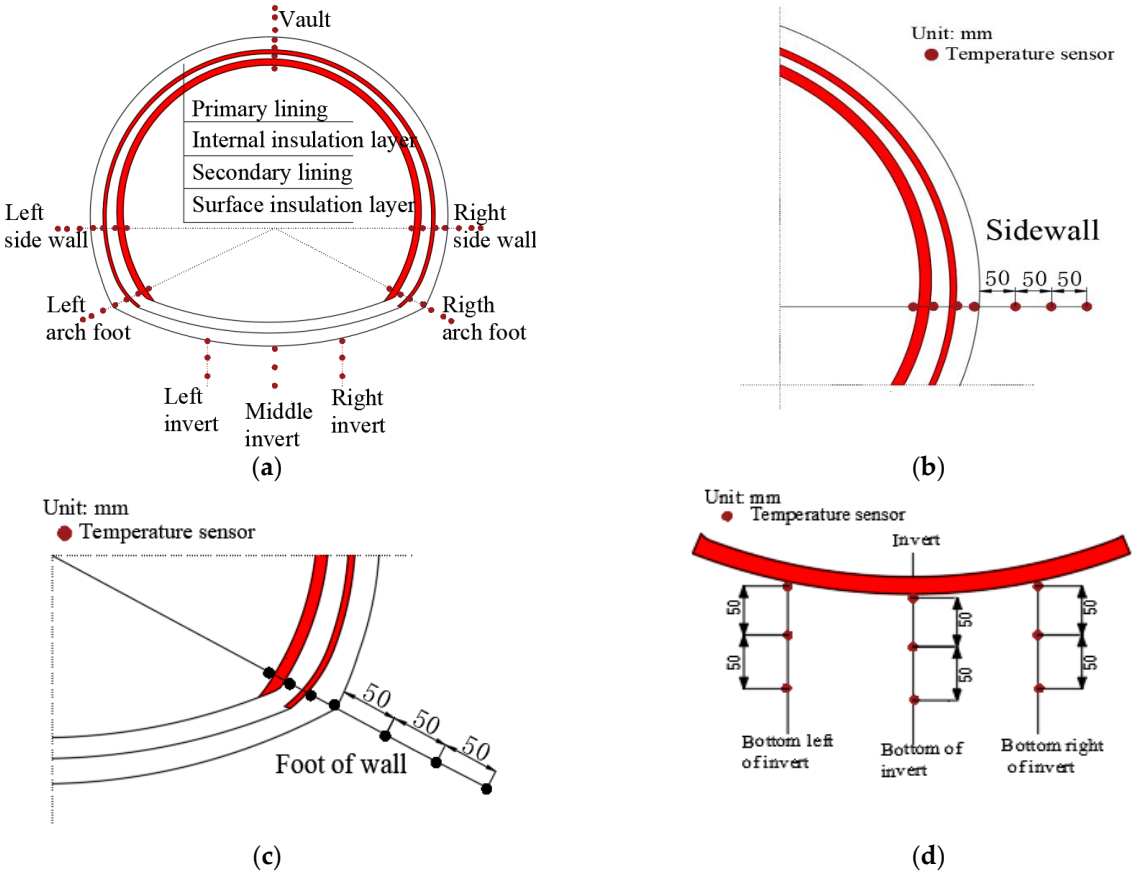


Figure 2. Schematic diagram of temperature sensor layout: (**a**) Layout position of tunnel cross section sensor; (**b**) Layout of side wall temperature sensor; (**c**) Layout of wall foot temperature sensor; (**d**) Layout of temperature sensor at inverted arch.

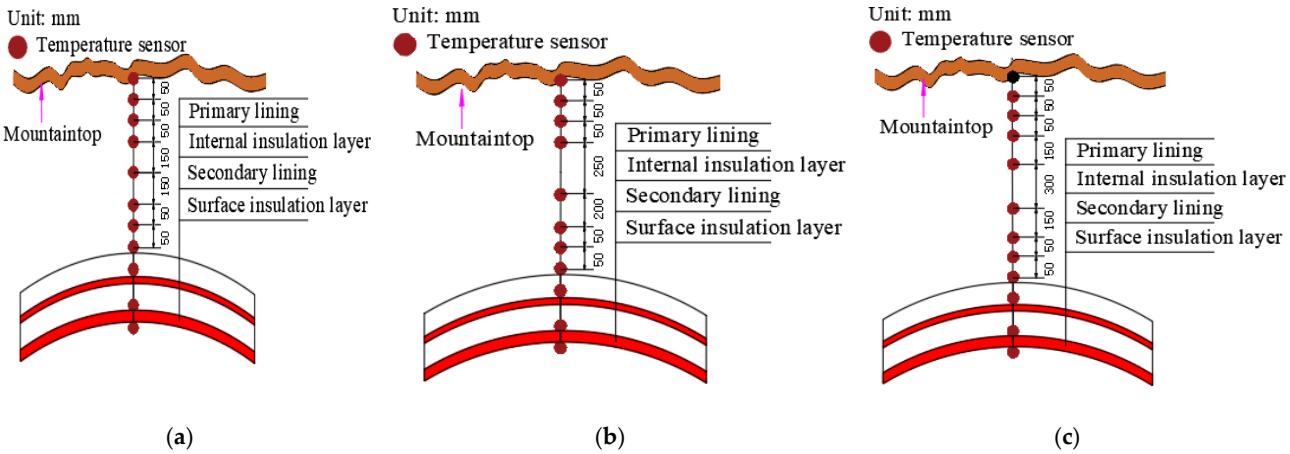


Figure 3. Layout of vault temperature sensor: (**a**) Section 1; (**b**) Section 2; (**c**) Section 3.

A total of 8 sections are set for temperature sensors in the model tunnel, and the distance between each section from left to right is 100 mm, 200 mm, 400 mm, 500 mm, 600 mm, 500 mm, 400 mm, 200 mm and 100 mm successively (see Figure 4). At the same time, Figure 5 shows the deployment of the wind speed sensor.

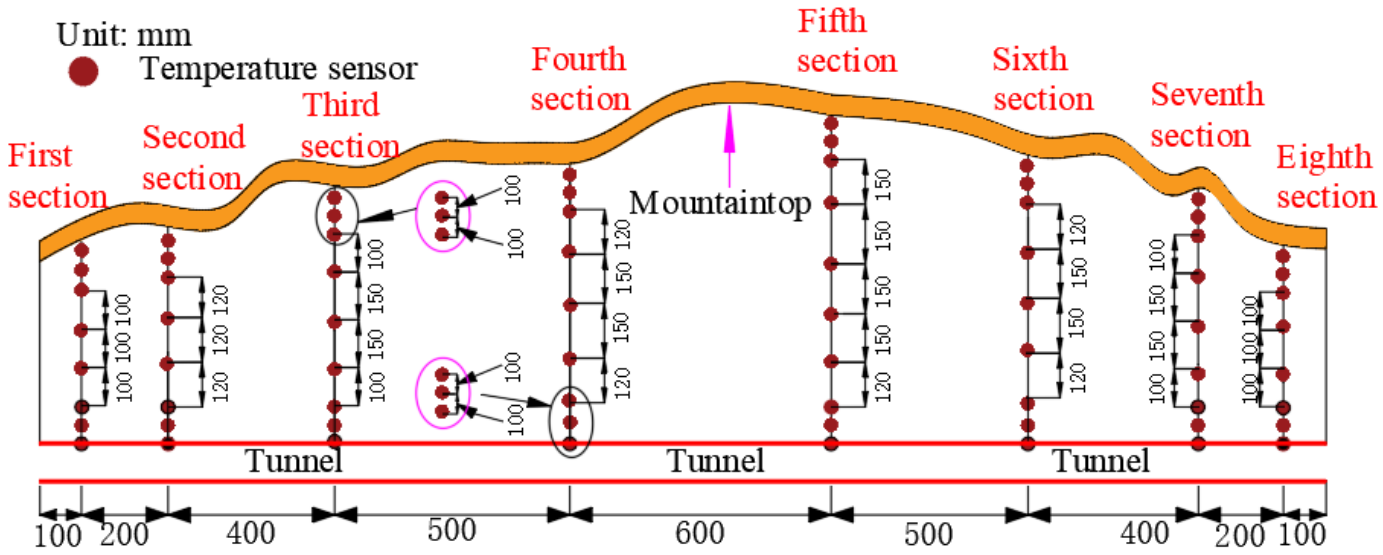


Figure 4. Layout diagram of tunnel longitudinal section temperature sensor.

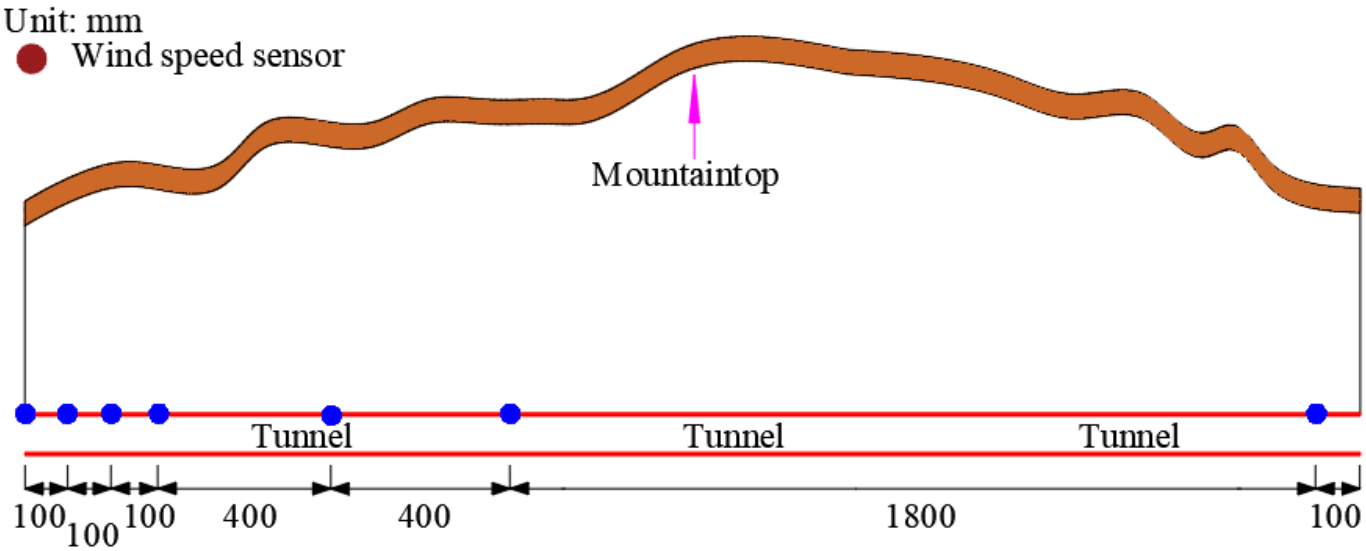


Figure 5. Schematic diagram of tunnel longitudinal section wind speed sensor layout.

2.3.3. Test Air Temperature and Ventilation Control Scheme

The ambient temperature is simulated through the alcohol circulation cold bath system. The temperature control is based on the measured results outside the Osaka Mountain Tunnel site during operation. Four temperatures (−2.4 °C, −4.8 °C, −8.4 °C, −10.6 °C) are selected as the ambient temperature for this model test. The ventilation circulation loop is established from the tunnel blowing hole to achieve the ventilation circulation state in the tunnel (See Figure 6).

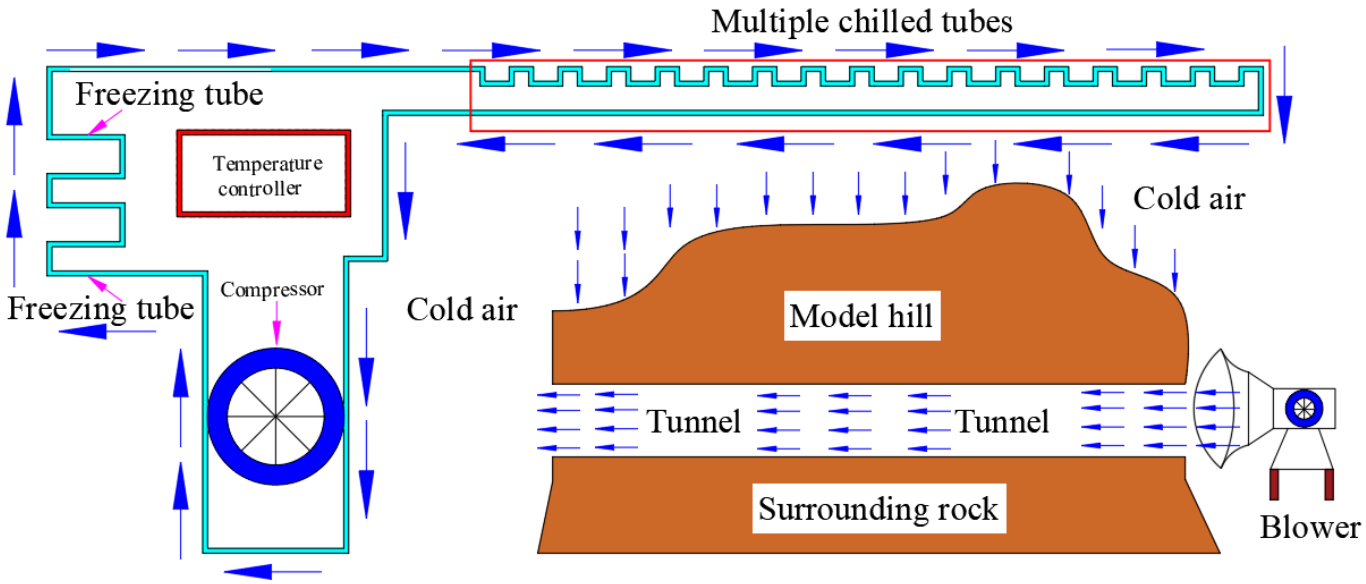


Figure 6. Working diagram of tunnel model freezing test system.

3. Experimental Results and Analysis

Based on the physical model test of alpine tunnels, the temperature and wind speed data under different working conditions are obtained. Under the conditions of both no ventilation and ventilation, the radial and longitudinal temperature distribution characteristics of the model tunnel are analyzed and the guiding significance of the model test to the site and the distribution characteristics of the expansion range of the tunnel freezing front are emphatically studied [28,29].

3.1. Characteristics of Radial and Longitudinal Air Temperature Distribution in Tunnels

3.1.1. Characteristics of Radial Air Temperature Distribution in Tunnels

Taking no ventilation as an example, the air temperature of −1.6 °C and −8.4 °C are selected to analyze the air temperature at different positions of tunnel sections 1, 3 and 5.

As can be seen from Figure 7, when the test air temperature is −1.6 °C, the overall temperature variation range of section 1, section 3 and section 5 are 0.9~13.3 °C, 2.2~15.0 °C and 11.2~19.0 °C, respectively, and the temperature variation at different locations of each section shows the same trend. The temperature on the surface of the insulation layer is the lowest and the variation trend is the highest. The temperature of the surrounding rock at a depth of 10 cm is the highest and the variation trend is the lowest. The farther the section is from the portal, the higher the temperature [30].

As can be seen from Figure 8, air temperature has a serious impact on the temperature inside the tunnel. When the test air temperature is −8.4 °C, the overall temperature variation range of section 1, section 3 and section 5 are −4.4~7.4 °C, −0.9~9.3 °C and 4.6~13.7 °C, respectively. The variation trend of air temperature at different positions of each section has the same variation trend as that of air temperature at −1.6 °C.

According to the above analysis, the temperature change of the tunnel wall (the surface of the insulation layer) is relatively strong. With the increase of the diameter depth, the temperature change of each position tends to moderate, and the temperature change in the surrounding rock is the most stable. These research results are consistent with those of Tan et al. (2014) [7]. Section 1 is located 10 cm from the tunnel entrance, which is close to the cold air mass outside the tunnel. The radial distance of the cold air along the insulation layer is relatively deep, and the temperature difference between the inner and outer walls of the insulation layer is smaller than that of other sections. The surrounding rock and lining are also affected by the cold air at the tunnel entrance side. Section 3 is located 70 cm from the entrance of the tunnel, which is far away from the cold air mass outside the tunnel.

Compared with section 1, the depth of cold air transferred along the radial direction of the insulation layer is reduced. Section 5 is 180 cm from the tunnel entrance and located in the middle of the tunnel. The temperature variation of section 5 is least affected by the cold air of the tunnel entrance.

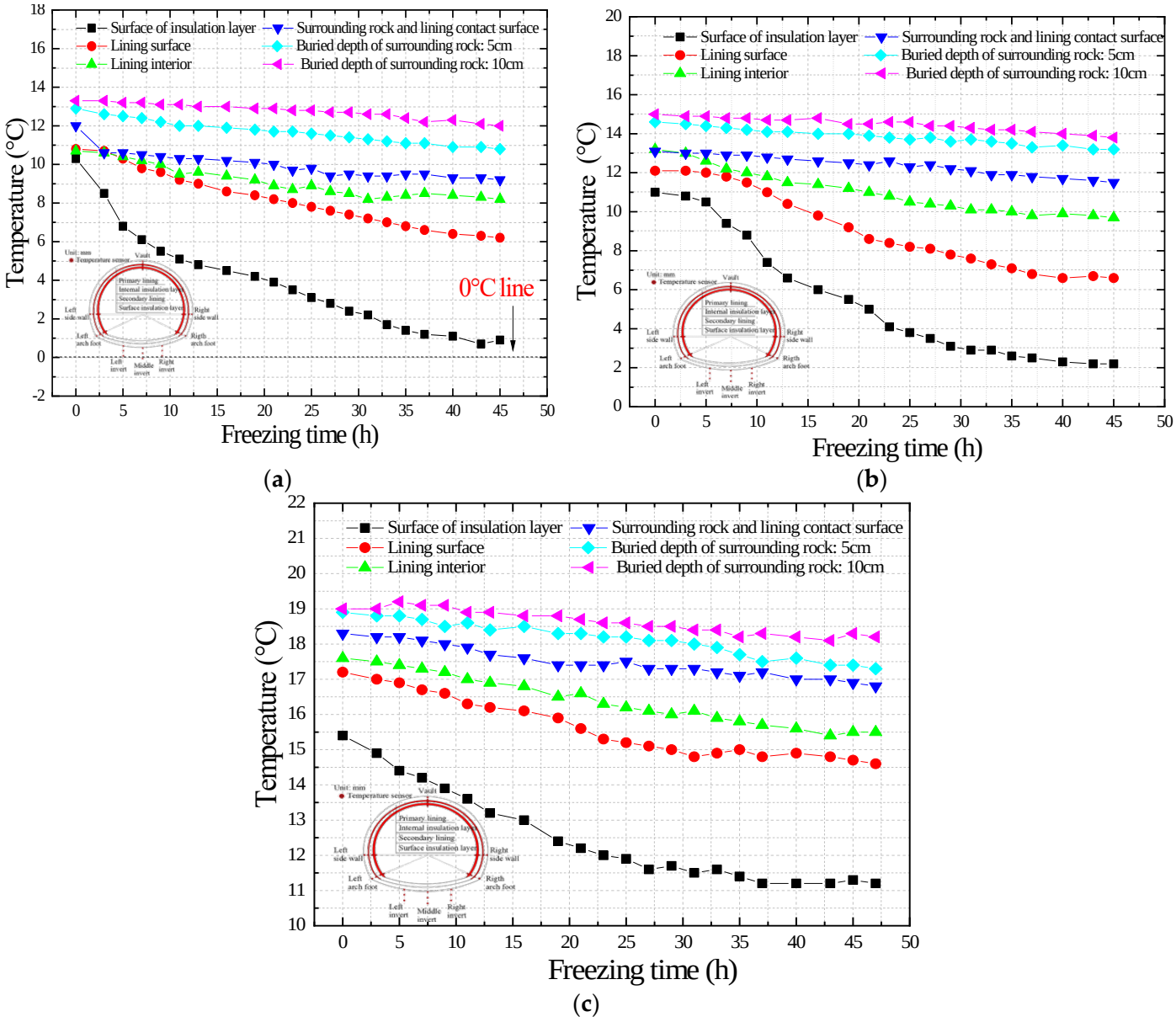


Figure 7. Temperature distribution at sections 1, 3 and 5 when the air temperature is −1.6 °C: (**a**) Section 1; (**b**) Section 3 (**c**) Section 5.

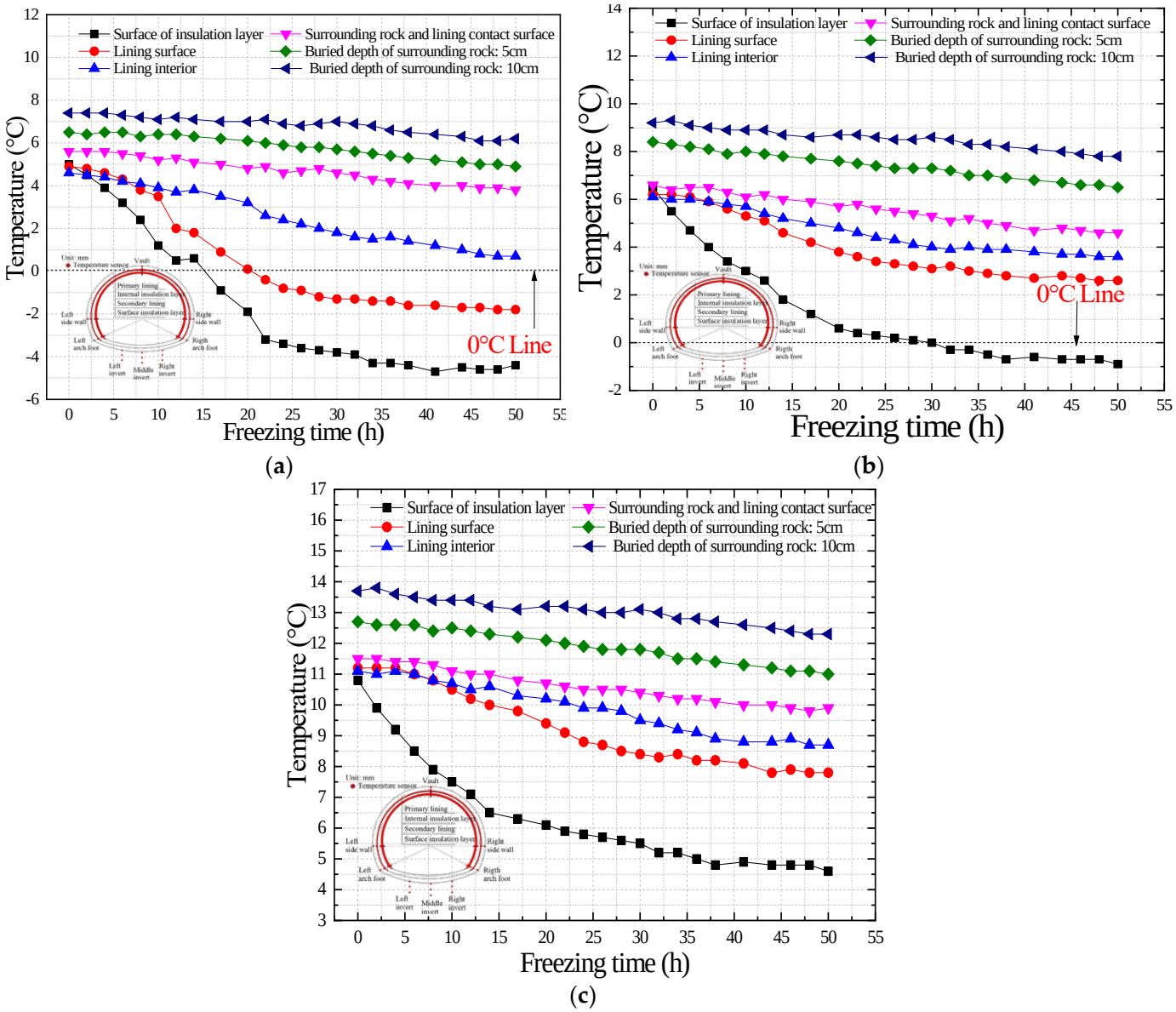


Figure 8. Temperature distribution at sections 1, 3 and 5 when the air temperature is −8.4 °C: (**a**) Section 1; (**b**) Section 3; (**c**) Section 5.

3.1.2. Characteristics of Longitudinal Air Temperature Distribution in Tunnels

Take air temperature of −1.6 °C, −4.8 °C, −8.4 °C, −10.6 °C, and ventilation conditions of 0 m/s, 1.8 m/s, 2.6 m/s, and 3.6 m/s, respectively, to analyze the characteristics of the longitudinal temperature distribution of the tunnel. The results are shown in Figure 9.

It can be seen from Figure 9 that the temperature curve in the tunnel from the inlet to the middle of the tunnel basically shows an upward trend, from the middle of the tunnel to the exit the temperature gradually decreases, and the temperature at both sides of the tunnel entrance and exit is lower than that at the center of the tunnel. When the test air temperature is −1.6 °C and −4.8 °C, the longitudinal air temperature curve in the tunnel assumes an inverted "V" shape [31]; when the test air temperature is −8.4 °C and −10.6 °C, the tunnel longitudinal air temperature curve shows a quadratic parabola variation. This shows that the lower the temperature is, the temperature curve tends toward linear variation from the tunnel entrance to the tunnel.

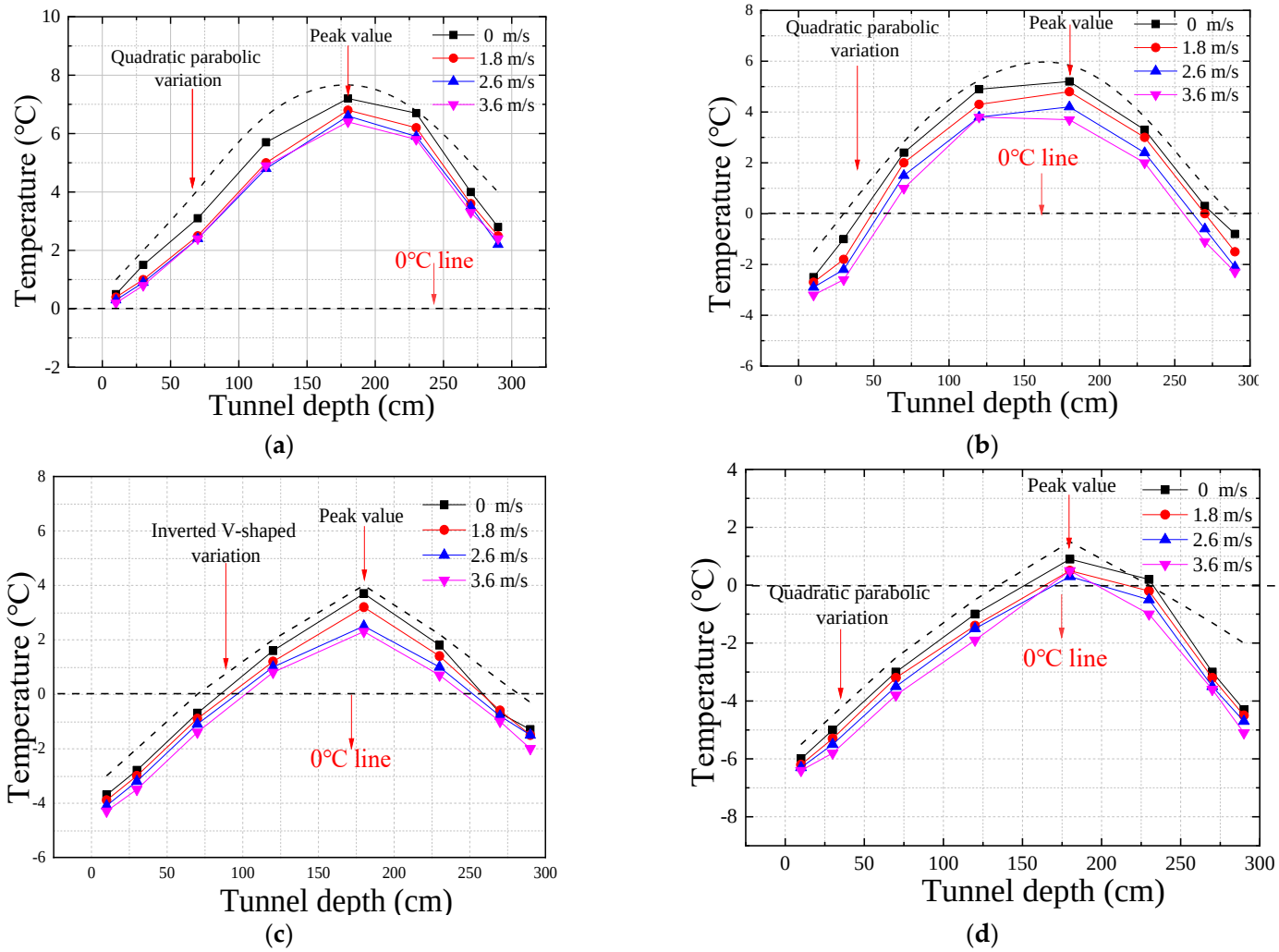


Figure 9. Temperature variation curve in tunnel under different test air temperature and different wind speed: (**a**) The temperature is −1.6 °C; (**b**) The temperature is −4.8 °C; (**c**) The temperature is −8.4 °C (**d**) The temperature is −10.6 °C.

3.1.3. Characteristics of Longitudinal Overall Temperature Distribution in Tunnels

Refer to the research method of Tan et al. (2014) [7]. Using the Surfer software, the cloud charts of the longitudinal overall temperature change of the tunnel are simulated when the temperature is −1.6 °C, −10.6 °C, and the wind speed is 0 m/s, 1.8 m/s.

It can be seen from Figure 10 that there is no freezing zone in the surrounding rock of the mountain, and only a small negative temperature zone exists at the tunnel entrance. At the wind speed of 1.8 m/s, we can definitively see that the cold air mass at the tunnel entrance extends to the inside of the tunnel.

It can be seen from Figure 11 that the top of the surrounding rock of the mountain, the surrounding rock of the portal lining and the surrounding rock of the inverted arch base of the portal all have different degrees of freezing areas. Under the wind speed of 3.6 m/s, the longitudinal increase distance of the 0 °C isotherm at the tunnel entrance reaches 35 cm, the longitudinal freezing length of the surrounding rock of the arch top reaches 85 cm, and the longitudinal freezing length of the surrounding rock of the inverted arch base reaches 135 cm.

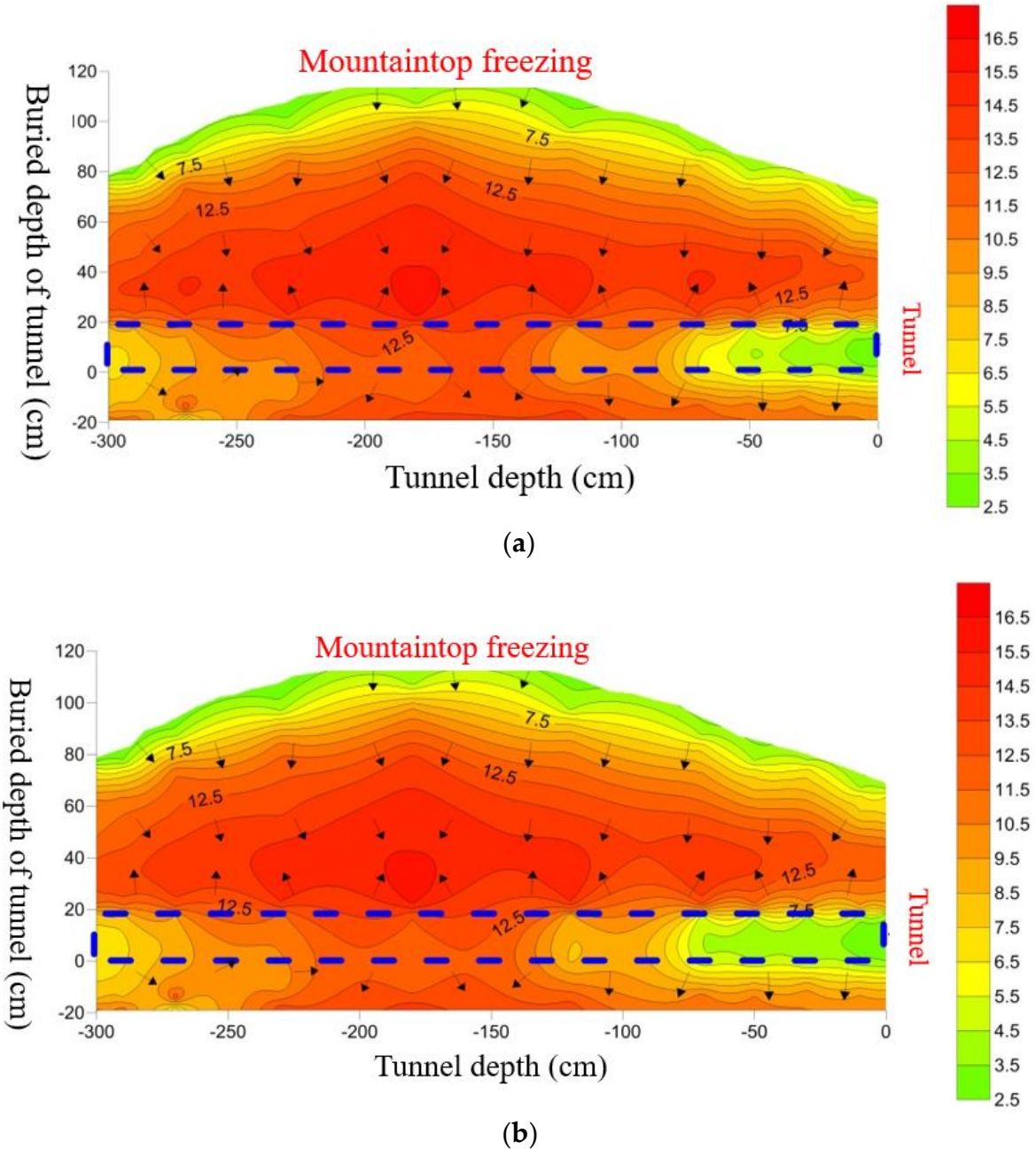


Figure 10. Vector Diagram of Tunnel Longitudinal Temperature Distribution at Test Air Temperature −1.6 °C: (**a**) 0 m/s; (**b**) 1.8 m/s.

It can be seen from the overall temperature distribution vector diagram of the tunnel that when the test air temperature is low, there is an obvious thermonuclear region in the surrounding rock of the mountain. As the test air temperature decreases, the thermonuclear region gradually shrinks, the surrounding-rock freezing area at the arch bottom gradually increases, and the surrounding-rock freezing area at the arch crown gradually expands to the inside of the mountain. Compared with no ventilation, the influence of ventilation on the longitudinal and radial temperature distribution of the tunnel is more obvious, and the greater the wind speed is the greater the influence is. In particular, the longitudinal temperature distribution of the tunnel is more widely affected by ventilation [32].

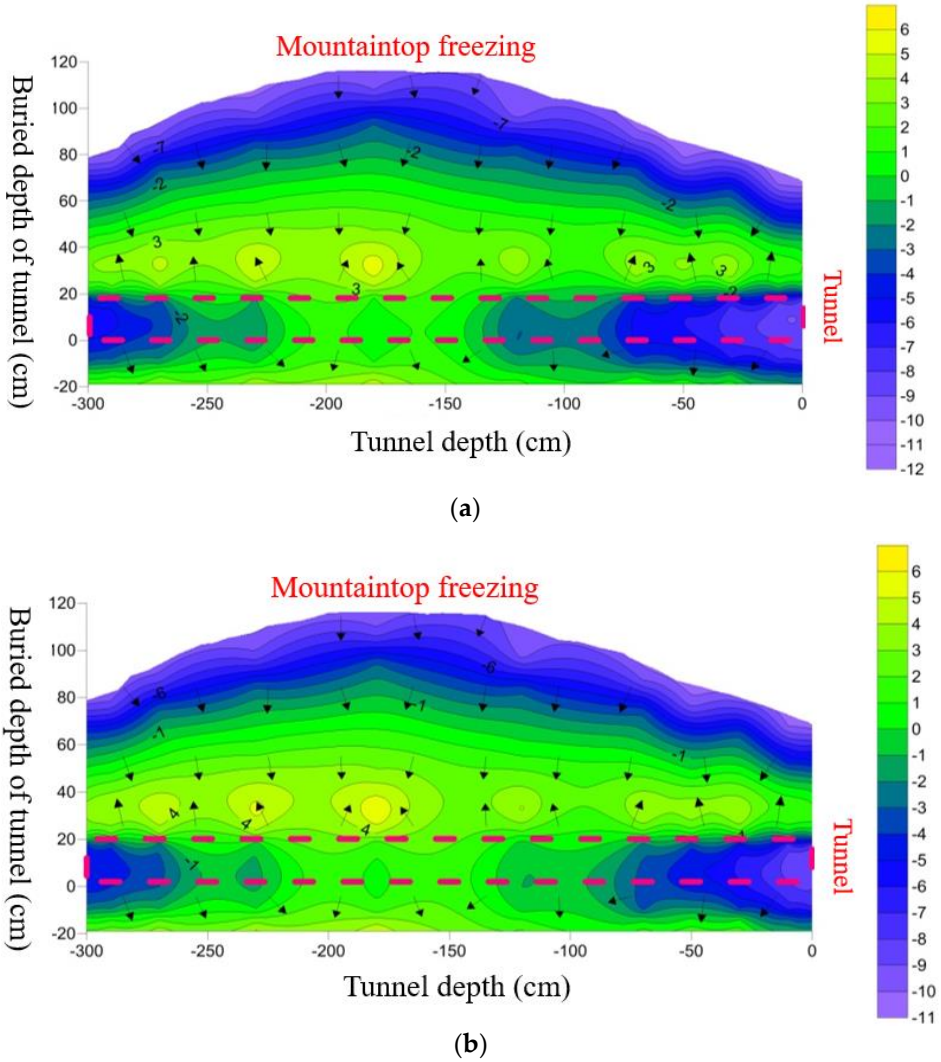


Figure 11. Vector Diagram of Tunnel Longitudinal Temperature Distribution at Test Air Temperature −10.6 °C: (**a**) 0 m/s; (**b**) 1.8 m/s.

3.2. Analysis of Freezing Front in Tunnel Model

Freezing front is an important parameter for analyzing and studying the surrounding rock freezing zone, so it is necessary to study it [33]. Assume that the freezing phase transition temperature is 0 °C. By extracting the 0 °C value at the vault, side wall, wall foot and inverted arch positions, the radial and longitudinal fitting analysis of the freezing front at each position is carried out. The control equation of the freezing front obtained has an important guiding significance for the radial and longitudinal uneven layout of the antifreeze insulation layer.

3.2.1. Radial Analysis of Freezing Front

The study of radial freezing front has important reference value for the radial non-uniform laying of an insulation layer. In the study, the insulation layer, lining and surrounding rock are considered as a whole. When it is stable, the tunnel radial 0 °C line is fitted. It can be seen from Figure 12 that the change rule of the tunnel radial freezing depth is basically in the form of a quadratic parabola function (under different function types, the fitting correlation coefficient of the quadratic parabola function is the highest). The distribution of freezing depth at different sections of the tunnel is similar. Section 1 (test air temperature −10.6 °C, wind speed 3.6 m/s at the entrance) is taken as the fitting analysis object of freezing front. As long as the distribution law of radial freezing front at

the entrance of the tunnel is obtained, the distribution characteristics of extending the range of radial freezing front at different sections can be determined along different longitudinal depths of the tunnel.

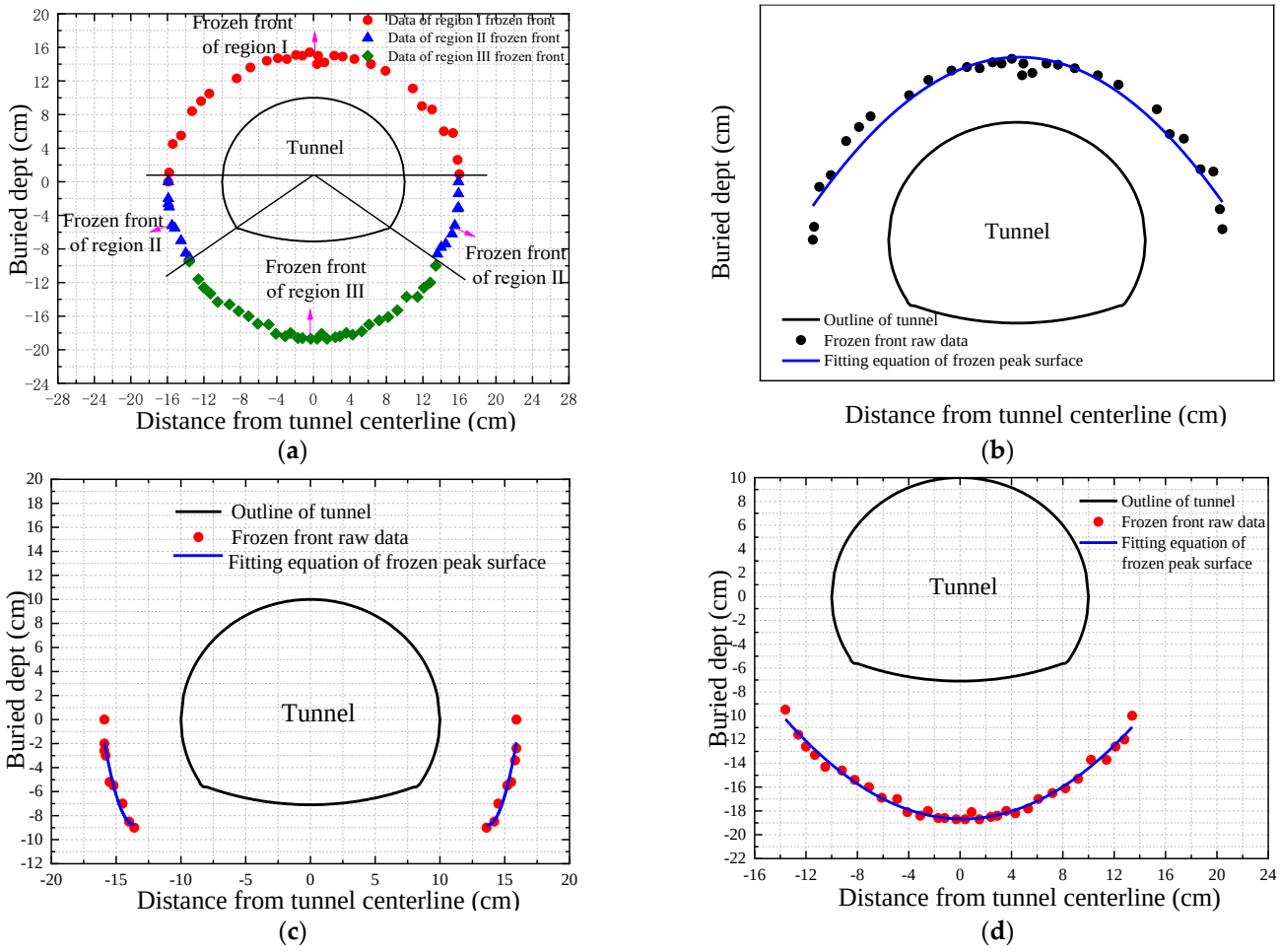


Figure 12. Fitting curve of frozen front in different regions: (**a**) Division area of frozen front; (**b**) Fitting curve of frozen front in Region I; (**c**) Fitting curve of frozen front in Region II; (**d**) Fitting curve of frozen front in Region III.

Due to the different distribution forms of the radial freezing front, in order to better analyze the tunnel radial freezing front it is divided into three regions (Region I, Region II and Region III), as shown in Figure 12a. The control curve thus obtained is more consistent with the distribution form of the freezing front in each region. Figure 12b–d show the fitting curve of the freezing front in the three regions. (By comparing the correlation coefficients of other types of function fitting equations, we see that the correlation coefficients of function fitting equations in Table 2 are the highest.)

Table 2. Governing equations of freezing front in different regions.

Region	Governing Equation	Correlation Coefficient
Region I	$y = 455.55e^{\frac{-(x-0.15)}{9144.93}} - 440.01$	0.9413
Region II	$y = 83.91e^{\lvert\frac{x}{0.87}\rvert} - 9.19$	0.9128
Region III	$y = 0.04x^2 - 0.002x - 18.67$	0.9794

Note: y in the table represents the buried depth of the tunnel; x is the distance from the tunnel centerline. Unit: cm.

It can be seen from the above three regional freezing front curves that the freezing front has reached a stable state, and the cold air in the tunnel makes the freezing front generate and move forward. At this time, there is no cold air to make the freezing front continue to move forward until the melting front reaches the location of the freezing front and stops. The freezing front will disappear outside the fitting curve, and a freezing thawing balance surface will appear.

The freezing front distance in Region III is the largest, mainly because the inverted arch is not paved with a thermal insulation layer, which means it lacks protection, and the concrete lining can easily be frozen through by cold air; the expansion distance of the freezing front at the foot of the wall in Region II is obviously higher than that of the freezing front at the vault in Region I, mainly because the cooler air is generally concentrated at the foot of the wall and the invert of the tunnel. The specific control equation of the frozen front is shown in Table 2.

In order to better fit the freezing front, three function types are used for fitting analysis. The correlation coefficients of the freezing front fitting functions obtained from the 3 regions are all above 0.9, indicating that the fitting effect is correct.

In conclusion, the freezing front at the inverted arch and the foot of the wall has the furthest expansion, followed by the side wall, and the vault has the least expansion. The inverted arch and the foot of the wall are the most dangerous positions of the whole section, and should be used as key thickening parts in the thermal insulation setting [34].

3.2.2. Longitudinal Analysis of Freezing Front

Only the fitting analysis of the radial freezing front can obtain the distribution form of the freezing region in a certain section, and the distribution form of the freezing front in continuous depth is missing. The research and analysis of the longitudinal freezing front has important guiding significance for longitudinal non-uniform laying of an insulation layer.

Since the range of freezing front at the tunnel entrance is larger than that at the tunnel exit, the freezing front at the tunnel entrance (test air temperature −10.6 °C, wind speed 3.6 m/s) is taken as an example for fitting analysis. Figure 13 is the schematic diagram of the longitudinal three-dimensional freezing front of the tunnel.

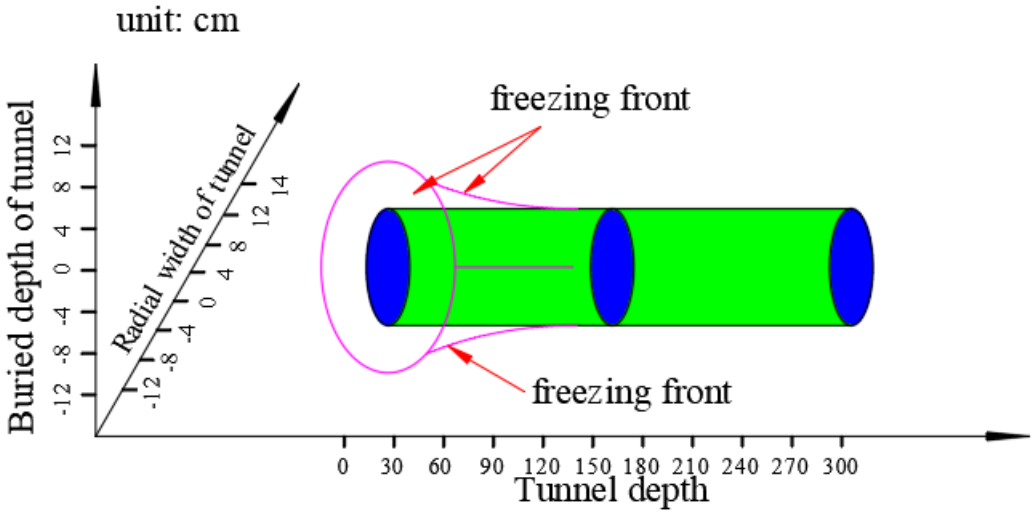
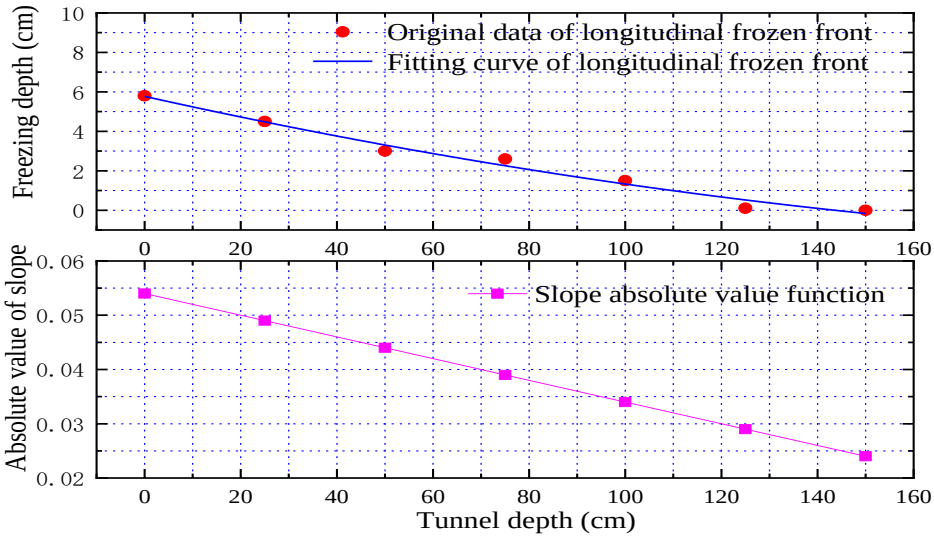
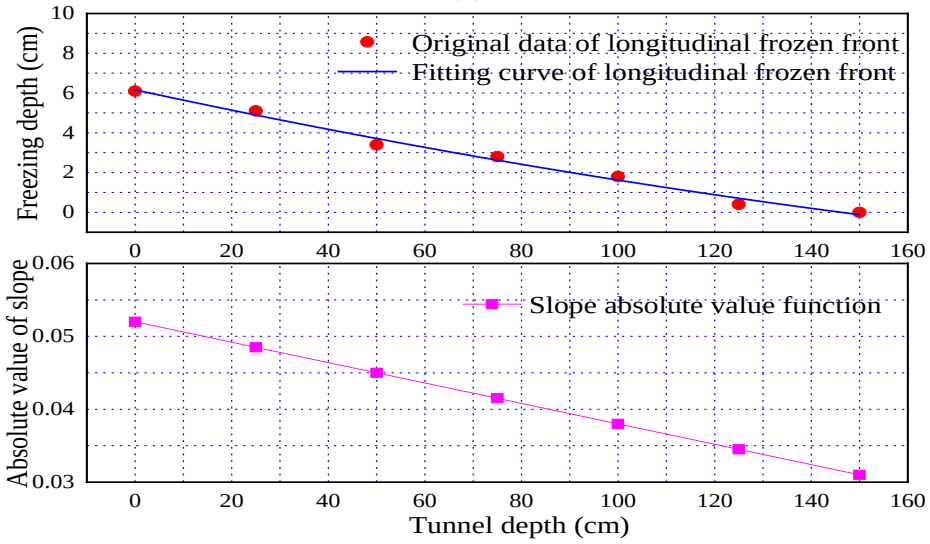


Figure 13. Three dimensional schematic diagram of longitudinal frozen front.

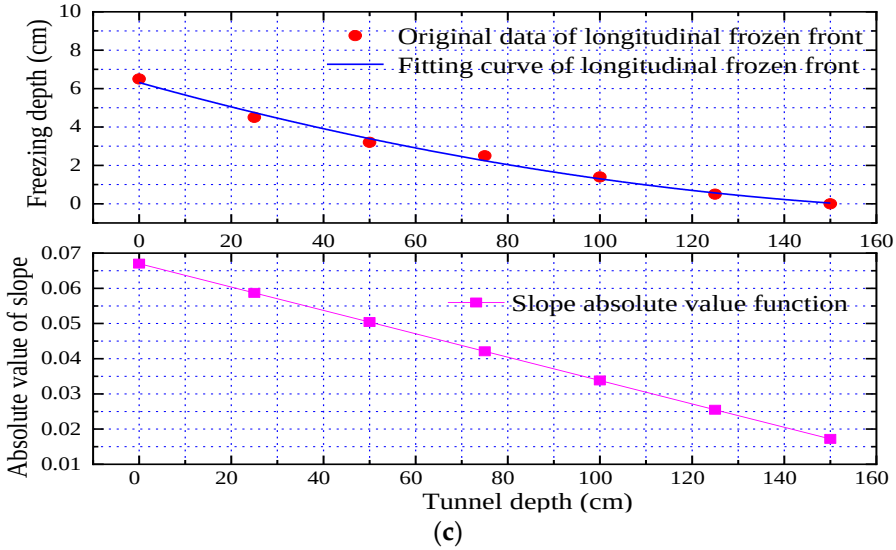
By extracting the values of the longitudinal freezing depth at different positions of the tunnel, the freezing area at the stable state of the 0 °C line was fitted, and the control curves of the longitudinal freezing front at different positions of the vault, side wall, foot of the wall and the vault were obtained, as shown in Figure 14. The fitting governing equation and correlation coefficient of the longitudinal freezing front at different positions are shown in Table 3.



(**a**)



(**b**)



(**c**)

Figure 14. *Cont.*

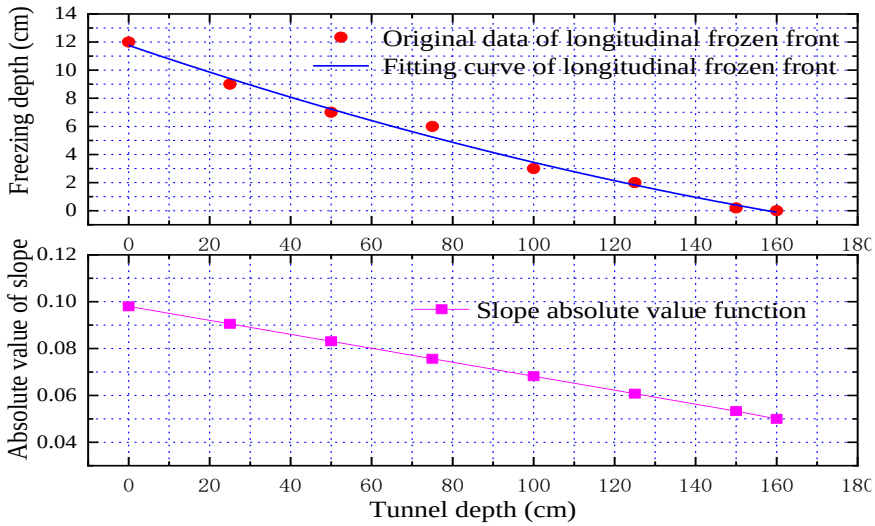


Figure 14. Fitting curve of longitudinal frozen front: (**a**) Vault; (**b**) Side wall; (**c**) The foot of the wall; (**d**) Inverted arch.

Table 3. Governing equations of longitudinal freezing front at different positions.

Position	Governing Equation	Correlation Coefficient
Vault	$y = 9.71 \times 10^{-5}x^2 - 0.054x + 5.77$	0.9898
Side wall	$y = 7.05 \times 10^{-4}x^2 - 0.052x + 6.16$	0.9762
The foot of the wall	$y = 1.66 \times 10^{-4}x^2 - 0.067x + 6.31$	0.9847
Inverted arch	$y = 1.49 \times 10^{-4}x^2 - 0.098x + 11.76$	0.9880

Note: y in the table is the freezing depth; x is the tunnel depth. Unit: cm.

The research method of Sun et al. is referred to when giving the control equation and analytical solution of freezing front [35,36].

It can be seen from Table 3 that the correlation coefficients of the 4 control equations are all above 0.97, indicating that the fitting effect is correct and can reflect the distribution characteristics of the tunnel longitudinal freezing front.

In summary, the longitudinal freezing front governing equation can be used to determine the extending distance of the longitudinal freezing front at different positions of the tunnel, and the specific distribution characteristics of the freezing area at different depth positions of the whole tunnel can be determined by combining the radial freezing front governing equation.

4. Conclusions

(1) With the decrease of the test air temperature, the thermonuclear region in the surrounding rock of the mountain gradually shrinks, the freezing area of the surrounding rock at the arch bottom gradually increases, and the freezing area of the surrounding rock at the arch crown gradually expands to the inside of the mountain; the influence of ventilation on the longitudinal and radial temperature distribution of the tunnel is more obvious, and the greater the wind speed is, the greater the influence is. In particular, the longitudinal temperature distribution of the tunnel is more widely affected by ventilation.

(2) The inverted arch is not paved with a thermal insulation layer, and so lacks protection. The lining concrete is easily frozen by cold air, leading to the maximum distance of the freezing front in the inverted arch area. The colder air gathers at the foot of the

tunnel wall and the invert, and the expansion distance of the freezing front at the foot of the wall is obviously higher than that at the vault.

(3) The control equations of the radial three zone freezing front and the longitudinal quadratic parabola of the tunnel model under ventilation conditions are determined. The change of the longitudinal freezing front at different locations of the tunnel is basically a parabola attenuation, and with the increase of tunnel depth the absolute value of the slope of the control curve decreases linearly, the change trend of the freezing front gradually eases and finally tends to be stable and disappear. Through this control equation, the specific distribution characteristics of the freezing front at different depths of the whole model tunnel can be predicted.

The research limit of this paper is the size effect of the model tunnel. The smaller model tunnel may affect the accuracy of mountain temperature transmission. In the future, research will focus on the influence of ventilation environments on the frozen front of large size tunnel models in cold regions.

Author Contributions: Conceptualization, L.L.; validation, J.Z.; writing—original draft preparation, Z.L. (Zhiqiang Li); supervision, Z.L. (Zhe Li). All authors have read and agreed to the published version of the manuscript.

Funding: China University Innovation Fund (2021DZ023); Weifang Science and Technology Development Plan (2021GX005).

Institutional Review Board Statement: Not applicable.

Informed Consent Statement: Not applicable.

Data Availability Statement: Not applicable.

Conflicts of Interest: The authors declare no conflict of interest.

References

1. Zhang, M.; Bi, J.; Chen, W.; Zhang, X.; Lu, J. Evaluation of calculation models for the thermal conductivity of soils. *Int. Commun. Heat Mass Transf.* **2018**, *94*, 14–23. [CrossRef]
2. Zhao, P.; Chen, J.; Luo, Y.; Li, Y.; Chen, L.; Wang, C.; Hu, T. Field measurement of air temperature in a cold region tunnel in northeast China. *Cold Reg. Sci. Technol.* **2020**, *171*, 102957. [CrossRef]
3. Inokuma, A.; Inano, S. Road tunnels in Japan: Deterioration and countermeasures. *Tunn. Undergr. Space Technol.* **1996**, *11*, 305–309. [CrossRef]
4. Okada, K.; Fujii, T. Icicle and frost heave prevention by adiabatic treatment in existing tunnel. In *Ground Freezing 97: Frost Action in Soils*; A.A. Balkema: Amsterdam, The Netherlands, 1997; pp. 461–467.
5. Sandegren, E. Insulation against ice railroad tunnels. *Transp. Res. Rec.* **1987**, *1150*, 43–48.
6. Zhou, X.; Zeng, Y.; Fan, L. Temperature field analysis of a cold-region railway tunnel considering mechanical and train-induced ventilation effects. *Appl. Therm. Eng.* **2016**, *100*, 114–124. [CrossRef]
7. Tan, X.; Chen, W.; Yang, D.; Dai, Y.; Wu, G.; Yang, J.; Yu, H.; Tian, H.; Zhao, W. Study on the influence of airflow on the temperature of the surrounding rock in a cold region tunnel and its application to insulation layer design. *Appl. Therm. Eng.* **2014**, *67*, 320–334. [CrossRef]
8. Andrén, A.; Dahlström, L.O.; Nordlund, E. Evaluation of a laboratory model test using field measurements of frost penetration in railway tunnels. *Cold Reg. Sci. Technol.* **2022**, *204*, 103660. [CrossRef]
9. Krarti, M.; Kreider, J.F. Analytical model for heat transfer in an underground air tunnel. *Energy Convers. Manag.* **1996**, *37*, 1561–1574. [CrossRef]
10. He, C.X.; Wu, Z.W. Preliminary prediction for the freezing–thawing situation in rock surrounding DabanShan tunnel. In *The Dissertations of the Fifth National Conference on Glaciology and Geocryology*; Culture Press of Gansu: Lanzhou, China, 1996; pp. 419–425.
11. He, C.; Wu, Z.; Zhu, L. A convection-conduction model for analysis of the freeze-thaw conditions in the surrounding rock wall of a tunnel in permafrost regions. *Sci. China Ser. D Earth Sci.* **1999**, *42*, 1–8. [CrossRef]
12. Lai, Y.M.; Liu, S.Y.; Wu, Z.W.; Yu, W.B. Approximate analytical solution for temperature fields in cold regions circular tunnels. *Cold Reg. Sci. Technol.* **2002**, *34*, 43–49.
13. Tang, G.; Wang, X. Effect of temperature control on a tunnel in permafrost. *Tunn. Undergr. Space Technol.* **2007**, *22*, 483–488. [CrossRef]
14. Zhang, X.; Xiao, J.; Zhang, Y.; Xiao, S. Study of the function of the insulation layer for treating water leakage in permafrost tunnels. *Appl. Therm. Eng.* **2007**, *27*, 637–645.

15. Zhou, X.; Ren, X.; Ye, X.; Tao, L.; Zeng, Y.; Liu, X. Temperature field and anti-freezing system for cold-region tunnels through rock with high geotemperatures. *Tunn. Undergr. Space Technol.* **2021**, *111*, 103843. [CrossRef]
16. Jain, P.K.; Singh, S. Analytical solution to transient asymmetric heat conduction in a multilayer annulus. *J. Heat Transfer.* **2009**, *131*, 011304. [CrossRef]
17. Lai, Y.M.; Wu, Z.; Zhu, Y.; Zhu, L. Nonlinear analysis for the coupled problem of temperature and seepage fields in cold regions tunnels. *Cold Reg. Sci. Technol.* **1999**, *29*, 89–96. [CrossRef]
18. Johansen, N.I.; Huang, S.L.; Aughenbaugh, N.B. Alaska's CRREL permafrost tunnel. *Tunn. Undergr. Space Technol.* **1988**, *3*, 19–24. [CrossRef]
19. Huang, S.L.; Aughenbaugh, N.B.; Wu, M.C. Stability study of CRREL permafrost tunnel. *J. Geotech. Eng.* **1986**, *112*, 777–790. [CrossRef]
20. Lunardini, V.J.; Varotta, R. Approximate solution to Neumann problem for soil systems. *J. Energy Resour. Technol.* **1981**, *103*, 76–81. [CrossRef]
21. Li, F.; Xia, M. Study on analytical solution of temperature field of artificial frozen soil by exponent-integral function. *Dongnan Daxue Xuebao/J. Southeast Univ.* **2004**, *34*, 469–473.
22. Jiang, B.S.; Wang, J.G.; Zhou, G.Q. Analytical calculation of temperature field around a single freezing pipe. *J. China Univ. Min. Technol.* **2009**, *38*, 463–466.
23. Zhou, Y.; Zhou, G.Q. Analytical solution for temperature field around a single freezing pipe considering unfrozen water. *J. China Coal Soc.* **2012**, *37*, 1649–1653.
24. Cai, H.; Liu, Z.; Li, S.; Zheng, T. Improved analytical prediction of ground frost heave during tunnel construction using artificial ground freezing technique. *Tunn. Undergr. Space Technol.* **2019**, *92*, 103050. [CrossRef]
25. Cai, H.; Peng, L.; Zheng, T. Prediction method of surface frost heave based on stochastic medium theory in tunnel freezing period. *J. Cent. South Univ.* **2014**, *45*, 4251–4257.
26. Liu, L.; Li, Z.; Liu, X.; Li, Y. Frost front research of a cold-region tunnel considering ventilation based on a physical model test. *Tunn. Undergr. Space Technol.* **2018**, *77*, 261–279. [CrossRef]
27. Cai, H.; Xu, L.; Yang, Y.; Li, L. Analytical solution and numerical simulation of the liquid nitrogen freezing-temperature field of a single pipe. *AIP Adv.* **2018**, *8*, 055119. [CrossRef]
28. Côté, H.; Thimus, J.F.; Rijkers, R.; Naaktgeboren, M. Soil behaviour during artificial freezing—Part 1: Frost heaving 3D tests. In *Ground Freezing 2000—Frost Action in Soils*; CRC Press: Boca Raton, FL, USA, 2020; pp. 69–74.
29. Katsurayama, H.; Abe, T. Thermochemical nonequilibrium modeling of a low-power argon arcjet wind tunnel. *J. Appl. Phys.* **2013**, *113*, 053304. [CrossRef]
30. Kiyanitsa, L.A.; Lugin, I.V.; Krasyuk, A.M. The Analysis of Thermal Conditions in Extra-Long Railway Tunnels during the Cold Season. *J. Min. Sci.* **2021**, *57*, 154–170. [CrossRef]
31. Han, J.; Fu, Z.; Li, B. Heat transfer model and temperature field distribution law of tunnel in permafrost region. *China J. Highw. Transp.* **2019**, *32*, 136.
32. Jun, K.J.; Hwang, Y.C.; Yune, C.Y. Field measurement of temperature inside tunnel in winter in Gangwon, Korea. *Cold Reg. Sci. Technol.* **2017**, *143*, 32–42. [CrossRef]
33. Zhao, X.; Zhang, H.; Lai, H.; Yang, X.; Wang, X.; Zhao, X. Temperature field characteristics and influencing factors on frost depth of a highway tunnel in a cold region. *Cold Reg. Sci. Technol.* **2020**, *179*, 103141. [CrossRef]
34. Feng, Q.; Jiang, B.S. Analytical method for insulation layer thickness of highway tunnels with multilayer dielectric in cold regions. *Chin. J. Geotech. Eng.* **2014**, *36*, 1779–1887.
35. Sun, Z.; Zhang, D.; Fang, Q.; Dui, G.; Chu, Z. Analytical solutions for deep tunnels in strain-softening rocks modeled by different elastic strain definitions with the unified strength theory. *Sci. China Technol. Sci.* **2022**, *65*, 2503–2519. [CrossRef]
36. Sun, Z.; Zhang, D.; Fang, Q.; Huangfu, N.; Chu, Z. Convergence-confinement analysis for tunnels with combined bolt–cable system considering the effects of intermediate principal stress. *Acta Geotech.* **2022**, 1–26. [CrossRef]

Disclaimer/Publisher's Note: The statements, opinions and data contained in all publications are solely those of the individual author(s) and contributor(s) and not of MDPI and/or the editor(s). MDPI and/or the editor(s) disclaim responsibility for any injury to people or property resulting from any ideas, methods, instructions or products referred to in the content.